Experimental measurements of the contribution of plasma turbulence to anomalous collision frequency in a Hall thruster

Zachariah A. Brown * and Benjamin A. Jorns†
University of Michigan, Ann Arbor, MI, 48109

The anomalous collision frequency that results from microturbulence in a Hall thruster plume is experimentally characterized. A combination of quasi-linear theory and measurements of ion density oscillations are employed to estimate an effective electron collision that results from the growth of the electron drift instability in the acceleration zone of a 9-kW class Hall thrusters. These values are compared to measurements of the actual electron collision frequency as inferred from an experimental technique based on laser induced fluorescence. In the near-field plume where the assumptions underlying the quasi-linear framework are satisfied, the wave-driven collision frequency is found to agree within experimental uncertainty with the measured collision frequency. However, the wave-driven effects are shown to over-predict the collision frequency in the thruster acceleration zone. These results suggest that while electron drift instability may be a dominant driver for anomalous transport in the Hall thruster, there may be limitations in applying the proposed quasi-linear framework to relate the measured wave properties to this transport. These results are discussed in the context of potential effects that may violate the quasi-linear assumption, including nonlinear wave-wave coupling and non-equilibrium electron distributions.

Nomenclature

B_0	=	Applied magnetic field
E_x	=	Applied electric field
g	=	Gordeev Function
j_e	=	Electron current density .
$k_{x,y,z}$	=	Wavenumber in the axial, azimuthal, and radial directions.
λ_{de}	=	Debye Length
L	=	Discharge chamber length
m	=	Electron mass
n_e	=	Electron density
ν_e	=	Total electron collision frequency
ν_c	=	Classical electron collision frequency
ν_{AN}	=	Anomalous electron collision frequency
ω_{ce}	=	Electron cyclotron frequency
q	=	Fundamental charge
ρ	=	Larmor radius
T_e	=	Electron temperature (eV)
u_i	=	Ion drift speed in axial direction
v_{de}	=	Electron drift speed in Hall direct

I. Introduction

The understanding of anomalous electron transport in Hall thrusters remains a significant challenge in the modelling and development of these devices. Hall thrusters employ crossed magnetic and electric fields to constrain electrons into an azimuthal Hall current to improve the residence time of electrons as they ionize a neutral gas propellant. Electrons are

*PhD Candidate , Department of Aerospace Engineering, AIAA Student Member
†Assistant Professor, Department of Aerospace Engineering, AIAA Associate Fellow

expected to travel across the magnetic field lines following classical particle-particle collision models, but experiments have demonstrated that the electron mobility is orders of magnitude higher than could be explained by collisions[1]. This so-called anomalous electron transport has yet to be adequately explained, which impedes efforts to model overall thruster operation and behavior which require an electron transport model [2].

Different theories have been proposed to explain this effect [3–8], but the emerging consensus points toward transport driven by the formation of coherent small-scale instabilities [9]. Recent kinetic simulations [10–16] and analytical models [17–19] suggest that the high azimuthal $E \times B$ velocity of the electrons results in the growth of the so-called electron drift instability (EDI). The EDI grows at the expense of electron kinetic energy and enhances the cross field mobility. While there have been several numerical and theoretical studies on this proposed transport mechanism, the experimental evidence has been more limited. Indeed, although recent experiments show the presence of this instability [20–23] in Hall thrusters, there has been no experimental data directly demonstrating that this instability results in the observed transport levels.

While we have recently demonstrated that the EDI could be solely responsible for observed transport level, the results were inconclusive due to missing information about the instability dispersion relation, which determines how much the oscillations in the plasma enhance transport [24]. Most notably, the wave-driven transport was shown to be extremely sensitive to the wavenumber along magnetic field lines, which was not directly measured. Additionally, mapping of wavenumber in the dispersion relation to experimentally measured frequencies was performed crudely and could have introduced significant uncertainty in the final result.

This work aims to resolve these previous issues through better determination of the radial wavenumber and implement a more refined technique for converting wavenumber to frequency space. To this end, the paper is organized as follows: In Section II we outline the plasma theory used to calculate the anomalous collision frequency. In Section III we detail the experimental setup and methodology. In Section IV. we present the results of the experiment and finally in Section V. the results are discussed.

II. Theory

In this section, we motivate a theoretical and experimental framework for inferring the anomalous collision frequency from the onset of low-level oscillations in the thruster plume. To this end, we first outline the problem of anomalous electron transport. We then introduce a formula for relating the properties of wave turbulence to an effective transport coefficient. Finally, we discuss methods for experimentally evaluating this expression for anomalous transport.

A. Problem of anomalous transport

Figure 1 shows a representative geometry of the Hall effect thruster. This cylindrical crossed-field device employs a radial magnetic field **B** that is perpendicular to an applied axial electric field **E** in order to confine electrons for efficient ionization. The magnetic field strength is selected such that while the electrons are strongly magnetized ($\rho_e << L$, where ρ_i is the electron Larmor radius and L is thruster channel length) and constrained to an $E \times B$ drift, the ions($\rho_i > L$) are not magnetized and freely stream out of the device. As a result, ions are accelerated electrostatically while in principle electrons are confined.

Due to particle-particle collisions, electrons should exhibit some small mobility across magnetic field lines in the direction of the electric field. However, due to the effect of some non-classical mechanism, the observed electron transport levels are orders of magnitude larger than could be explained by collisions. Most recent efforts to explain this cross-field transport phenomenon have focused on how the formation of microscale instabilities propagating in the $E \times B$ direction could increase cross-field transport.

B. Relating properties of plasma turbulence to transport

The onset of electrostatic fluctuations can promote cross-field transport levels that exceed the classical value. We can represent this impact by introducing an anomalous force R_{an} to the electron momentum equation:

$$\frac{\partial(mn\vec{v}_e)}{\partial t} + \nabla \cdot (mn\vec{v}_e\vec{v}_e) = -qn(\vec{E} + \vec{v}_e \times \vec{B} - \nabla(nT_e) - mn\nu_c\vec{v}_e + \vec{R}_{an}. \tag{1}$$

Here m is electron mass, n is electron density, $\vec{v}_e$ is the electron velocity, E and B are externally applied electric and magnetic fields, and ν_c is the classical electron collision frequency. Following the quasi-linear techniques of Davidson and Krall[25], the anomalous force term can be represented by the phase-averaged interaction between electric field and

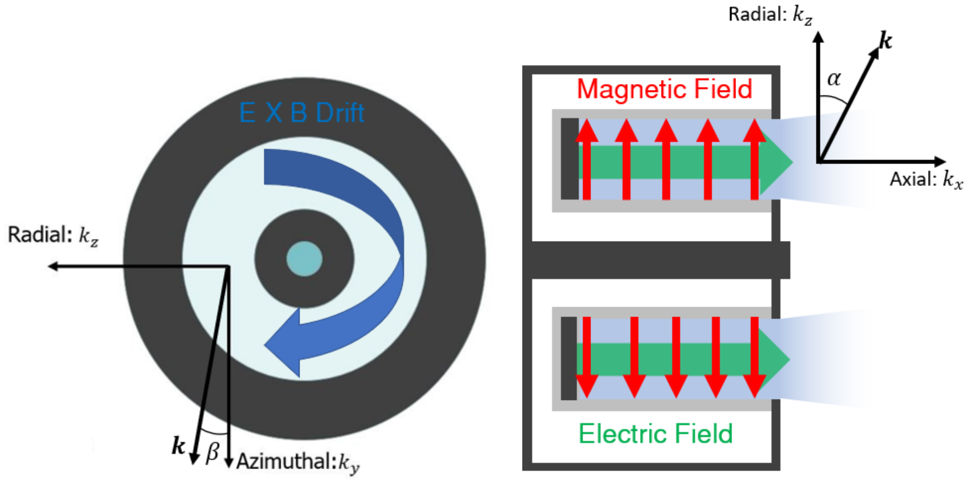

Fig. 1 Schematic of a Hall thruster with the wave direction coordinate system. The components are k_x along the electric field vector, k_y in the $E \times B$ direction, and k_z along the magnetic field lines.

density perturbations in the azimuthal direction and related to an effective collision frequency (ν_{an}) by

$$R_{an} = -e\langle \delta E \delta n \rangle = -mn\nu_{an} V_{E\times B} \tag{2}$$

$$\nu_{an} = \frac{e}{mnV_{E\times B}} \langle \delta E \delta n \rangle = \omega_{ce} \frac{\langle \delta E \delta n \rangle}{nE_x}. \tag{3}$$

Here the perturbations terms denoted by δx are fast oscillations about some mean value $\bar{x}$, $V_{E\times B}$ is the electron velocity in the azimuthal direction driven by the crossed axial electric and radial magnetic fields ($V_{E\times B} = E_x/B_r$), and ω_{ce} is electron cyclotron frequency. The brackets here indicate taking the phase average of the terms inside. If electric field and density oscillations are in-phase, this phase averaged term will be non-zero and result in an effective force.

In order to evaluate the anomalous collision frequency, we need measurements of the density and electric field perturbations. However, while measurements of local density oscillations are simple to collect, the same is not true of local electric field oscillations. In lieu of direct electric field oscillations, if we know the type of instability that is present in the plasma, we use its dispersion relation to relate the electric field amplitude to the density measurements. Simulations have shown the electron drift instability is most likely to form and result in the cross field transport. This drift-driven instability develops due the high azimuthal electron velocity against the relatively stationary ions. The instability grows at the expense of the electron kinetic energy and acts as an effective drag force.

With this in mind, following the work of Ducrocq et al. and Cavalier et al.[17, 18], the dispersion relation for the Hall thruster geometry (Fig. 1) is given by

$$1 + k^2\lambda_{De}^2 + g\left(\frac{\omega - k_y V_{E\times B}}{\omega_{ce}}, (k_x^2 + k_y^2)\rho^2, k_z^2\rho^2\right) - \frac{k^2\lambda_{De}^2\omega_{pi}^2}{(\omega - k_x V_b)} = 0, \tag{4}$$

where g(Ω, X, Y) is the Gordeev function, defined as

$$g(\Omega, X, Y) = i\Omega \int_0^{+\infty} e^{-X[1-cos(\varphi)]-\frac{1}{2}\varphi^2+i\Omega\varphi} d\varphi. \tag{5}$$

Here ω is the complex oscillation frequency, ω_{ce} is the electron cyclotron frequency, ω_{pi} is the ion plasma frequency, $k = \sqrt{k_x^2 + k_y^2 + k_z^2}$ is the oscillation wavenumber, k_x is the wavevector component traveling in the axial direction, k_y is the component in the $E \times B$ direction, k_z is the component in the radial direction (along magnetic field lines), V_{Dey} is the azimuthal electron drift velocity, V_b is the ion beam velocity in the axial direction, λ_{De} is the Debye length, and

$\rho = V_{the}/\omega_{ce}$ is the electron Larmor radius at thermal velocity $V_{the} = \sqrt{qT_e/m}$ where T_e is expressed in electron-volts. Following this dispersion relation density perturbations can be related to plasma potential oscillations by:

$$\delta\phi = \frac{\delta n}{n} T_e \frac{1 + g_r - i g_i}{(1 + g_r)^2 + g_i^2}, \tag{6}$$

where g_r and g_i are the real and imaginary components of the Gordeev function respectively. Finally, we assume the potential perturbations can be represented by a Fourier decomposition and are related to the electric field perturbations by

$$\delta\phi = \sum_{k_y} \tilde{\phi}_{(k_y)} e^{i(k_y y - \omega t)} + \text{c.c.} \tag{7}$$

$$\delta E = -\nabla\phi = -i k_y \delta\phi, \tag{8}$$

where c.c. denotes the complex conjugate and $\tilde{\phi}_{(k_z)}$ is the complex amplitude at wavenumber k_y. With these relations, the anomalous collision frequency is given by

$$\nu_{AN} = \omega_{ce} \frac{< \delta n_e \delta E_y >}{n_e E_x} = \frac{\omega_{ce}}{E_x} T_e \sum_{k_y} \left[k_y \left(\frac{|n_{k_y}|}{n} \right)^2 \frac{-g_i}{(1 + g_r)^2 + g_i^2} \right]. \tag{9}$$

The Gordeev function related term $g_i/(1 + g_r)^2 + g_i^2$ is a proxy for the growth of the instability at a particular wavenumber. Therefore this equation shows that the anomalous collision frequency will be high when both the oscillation amplitude ($|n_k|/n$) is large and the oscillations coincide with wavenumbers of high growth from the dispersion. Alternatively, if a measured oscillation is strong at a particular frequency, but that frequency does not map to high growth rate, then it will not strongly contribute to enhanced transport.

C. Inferring wavenumber spectrum of fluctuations

In practice, as we describe in the next section, nearly all the background plasma state variables in Eq. 9—electron temperature, density, electric field, and magnetic field — can be measured. In principle, the spectrum of density fluctuations as a function of wavenumber, n_{k_y} also can be inferred. For example, measurement with coherent Thomson scattering[26] can directly determine this quantity, while we previously have used Beall analysis combined with ion saturation probes to infer this property[23, 24]. However, there are limitations with both techniques. While the collective Thomson scattering technique can directly determine $|n_k|/n$, it is limited in the wavenumber space it can access. This technique can only see part of the spectrum at high wavenumber, and notably did not detect a local maximum in oscillation amplitude within the wavenumber domain. This implies that the wavenumbers with the highest amplitudes and perhaps strongest contribution to transport could not be seen. Alternatively, the probe-based technique can only access small wavenumbers relative to where the maximum growth is expected, but it can measure the entire frequency domain expected of the EDI.

In light of these limitations, we instead work in frequency space when evaluating the anomalous collision frequency. We measure the time-resolved fluctuations in the plasma and apply a Fourier transform. This yields the power spectrum as a function of frequency, $|n_\omega|$. If the dispersion relation $\omega(k_y)$ is known, we thus can in principle can invert it to transform $|n_\omega| \to |n_{k_y}|$. The challenge with this approach, however, is the EDI dispersion relation (Eq. 4) is not necessarily a one-one function between frequency and wavenumber. Therefore, we must employ a method for assigning an effective wavenumber and value of the Gordeev function at each frequency.

An example dispersion relation for the EDI in the Hall thruster acceleration zone in shown in Figure 2. The growth rate is peaked at multiple discrete wavenumbers corresponding approximately to harmonics of the electron cyclotron resonance frequency: $k_y = n\omega_{ce}/V_{E\times B}$, where n in the harmonic mode number. The real frequency at each harmonic is centered in periodic regions of high $d\omega/dk_y$. Outside the harmonic, the slope of real frequency turns negative before leveling out and then turns positive again approaching the next harmonic. It is in this region between the harmonics where the dispersion relation no longer is a one-one function between frequency and wavenumber.

In order to make a one-one function we first use our calculated dispersion relation to create map between frequency and the dispersion related term in Eq. 9: $-k_y \frac{g_i}{(1+g_r)^2+g_i^2}$, which is also not a one-one relation. We then create bins in the frequency domain and assign to each bin the average value of $-k_y \frac{g_i}{(1+g_r)^2+g_i^2}$ within the frequency range. An example of

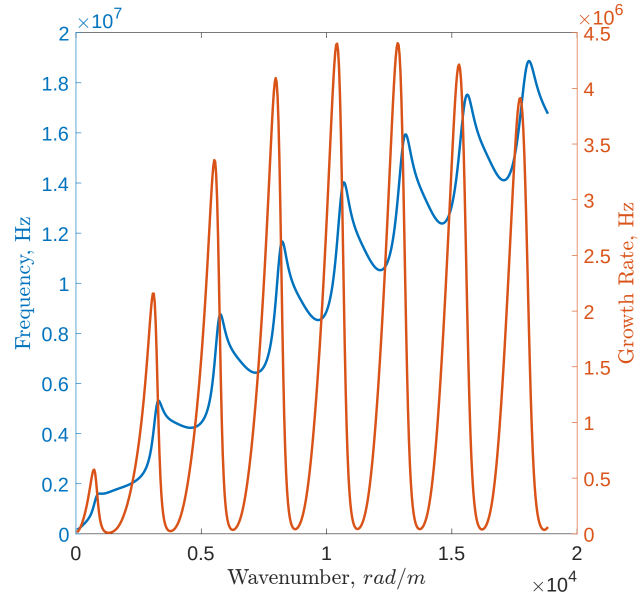

Fig. 2 Representative dispersion relation of the EDI the Hall thruster plume. Real frequency (blue) and growth rate (orange) are plotted against the azimuthal wavenumber k_y.

this process is shown in Fig. 3 where we use the results of the sample dispersion relation in Fig. 2. Here the impact of the discrete peaks in growth rate is retained, albeit with noise that depends on both the width of the frequency bin and the wavenumber resolution used when solving the dispersion relation. As discussed in the Sec. I, this approach of mapping frequencies to wavenumber is a substantial improvement over the previous methodology used in Ref[24] where the averaging was effectively done over the entire frequency space and reduced to a constant value. This earlier approach largely ignored the discrete nature of the dispersion relation.

III. Experimental Setup

A. Test article

All data for this experiment was collected using the H9, a 9-kW class Hall effect thruster developed jointly by NASA's Jet Propulsion Laboratory, the University of Michigan, and the Air Force Research Laboratory [27, 28]. The H9 employs a magnetically shielded topography [29], and uses a center-mounted LaB_6 hollow cathode. This thruster was tested in the Large Vacuum Test Facility (LVTF) at the University of Michigan. The H9 was operated at 300V and 15A with a xenon flow rate of 165 sccm through the anode and a 7% cathode flow fraction. The thruster body was electrically tied to the cathode.

The experimental layout for characterizing the H9 is shown in Fig.4 with the key diagnostics shown: wave measurement probes and laser optics for laser induced florescence (LIF) measurement of the beam ions. The wave probes are used to determine the power spectrum of ion density oscillations at various positions in the plume, and the LIF measurements are used to estimate local plasma parameters and provide a baseline anomalous collision frequency.

B. LIF setup for inferring background plasma properties

Following the works Perez-Luna and Dale, we determine plasma density, electric field, electron temperature, ion beam velocity, and anomalous collision frequency non-invasively through laser-induced fluoresence (LIF) measurements[30, 31]. LIF is used to measure the axial ion velocity distribution function at multiple locations along channel centerline from the thruster exit plan to almost a channel length down stream. The ion velocity distribution function (VDF). can then be used to solve the one-dimensional Boltzmann equation for density, temperature and electric field when combined with a downstream boundary condition for density. This downstream density is estimated using the wave probes which are biased far into the ion saturation current regime. The electron collision frequency can

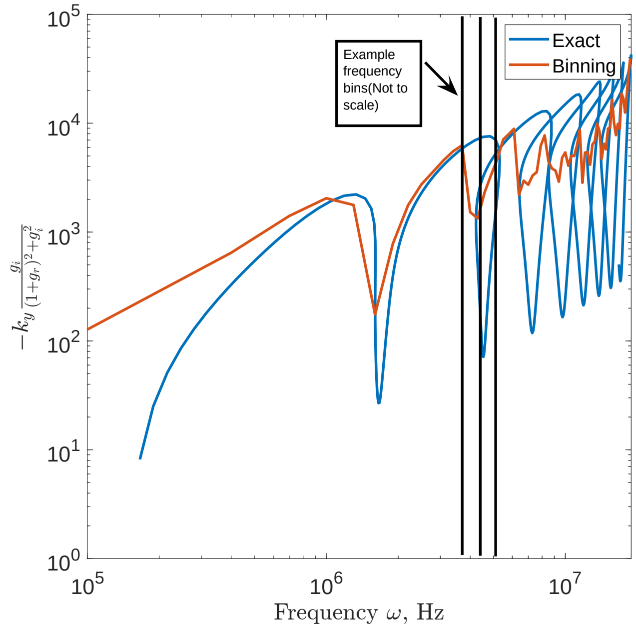

Fig. 3 Demonstration of the binning technique used to generate a one-one relationship between frequency and wavenumber. The raw value of $-k_y\frac{g_i}{(1+g_r)^2+g_i^2}$ is plotted against frequency in blue while the binned function is shown in orange with example frequency bins (not to scale).

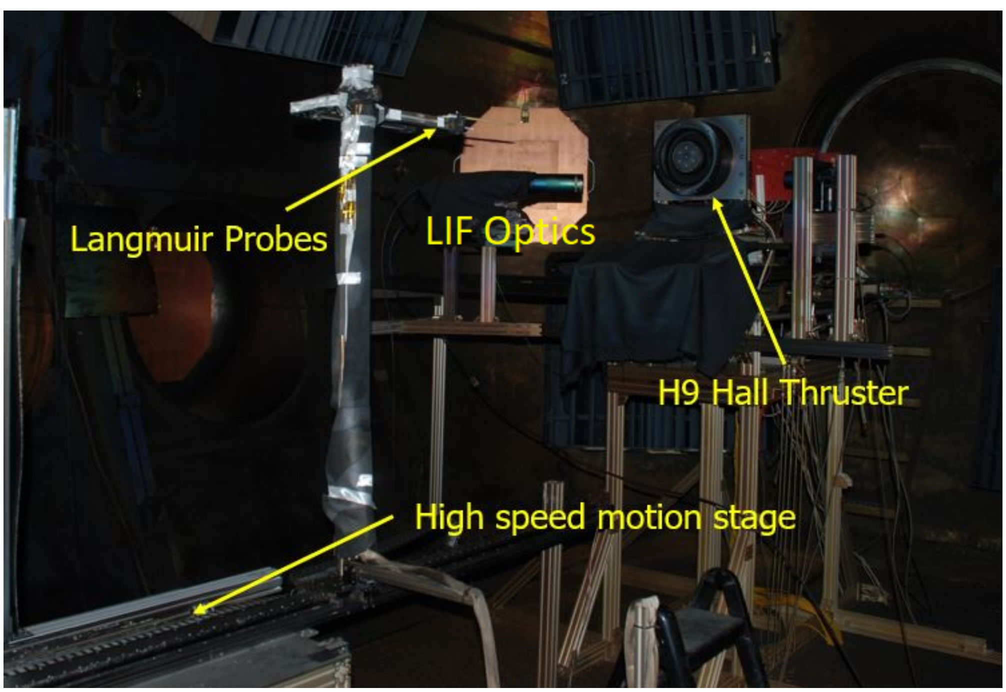

Fig. 4 H9 Hall thruster installed in LVTF with LIF optics and wave probes.

be calculated using the electron momentum equation as described in Ref. [31]. The LIF results in this paper were previously published in Ref.[24] and are repeated here for completeness with only the density and electron collision frequency being slightly changed due to more precise estimation of downstream density compared to the previous work.

C. Ion saturation probes

We employed ion saturation probes for measuring the fluctuations in ion density. These cylindrical probes were oriented in the x direction, parallel to the ion beam, to minimize the effect of ram current and mounted on fast motion stages to quickly the inject the probes in the plume and minimize perturbative effects. The probes collected data at fixed locations along channel centerline that overlapped with the LIF data-set with spatial uncertainty of ±2mm due the length of the probe tips.

The ion saturation probes are biased to -45V using batteries. The current is read across a low-inductance and low-capacitance 100Ω resistor into a ATS9462 16-bit digitizer. The fluctuations in ion saturation are then related to fluctuations in plasma density by $\tilde{i}_{sat}/\bar{I}_{sat} = \tilde{n}/\bar{n}$ where we have assumed electron temperature oscillations are negligible. Here we assume quasi-neutrality has the electron and ion density oscillation amplitudes to be roughly the same magnitude.

By performing a Fourier analysis, we can determine the power spectrum $|n_\omega|/n$, and by using the cross-correlation between two probe signals we can estimate the wavenumber of the oscillation. As discussed in the previous section, these probes can only directly measure the low wavenumber domain. The largest directly measurable wavenumber is $\pi/\Delta x$, where Δx is the spacing between the probes. In total there were 3 probes, with one pair being offset in the axial direction by 1 cm and another in the radial 1.5 cm.

IV. Results

In this section we present the results of our investigation, starting first with plasma parameters determined from the LIF technique and then the wave estimated collision frequency. Here we will also provide a brief discussion on the sources of uncertainty in each diagnostic.

A. Background plasma properties

The main four plasma parameters inferred from LIF, ion velocity, electron temperature, electric field strength, and plasma density are shown in Figure 5 as a function of position in the plume with z/L denoting the exit plane of the thruster. The majority of the ion acceleration occurs in just a narrow region downstream at $z/L \approx 1.1$ which is commensurate with the peak electric field observed at this location and a narrow peak in electron temperature. As described in Ref[31] the LIF-Boltzmann integration technique only directly yields the normalized density gradient ($\nabla n/n$), In order determine the density profile a downstream density measurement is needed to anchor the integration. For this we used the mean ion saturation current from the wave probes. This yielded a plasma density between $2 - 3 \times 10^{17}$ m^3 at the end of the LIF domain. The density profile shown in Figure 5 represents the range of densities that can occur at each location in the domain due the uncertainty in the downstream measurement.

B. Dispersion relation

The measured radial and axial dispersion relation are shown in Figures 6 and 7 as Beall plots. Beall plots are effectively histograms in frequency and wavenumber where the counts are the power spectrum at that frequency and wavenumber combination [32]. The radial dispersion shows several blob-like structures at the frequencies corresponding to the EDI resonant frequencies and wavenumbers on the order of 50-150 rad/m. The axial dispersion shows substantial structure in frequency domain belonging to the EDI. The Beall plots exhibit substantial phase wrapping where the dispersion relation appears continually wrap around the edge of the figure, which is indicative of oscillation wavenumbers larger than can be directly measured due to the finite probe spacing. We highlight this effect in Fig. 8 where we have repeated the Beall plot in wavenumber space to demonstrate the continuous structure. This unwrapped structure is very similar to the example dispersion relation shown in Figure 2 where the parts of the dispersion that were not one-one relations were smoothed over in the experimental data. This very clear axial data allows for a second method of estimating the radial wavenumber. The slope of the dispersion relation near the resonance harmonics is strongly related to the value of the radial wavenumber. By iterating on the radial wavenumber in our calculation of the theoretical dispersion, we can find what values gives the closest match to the slope seen in the Beall plots. The value determined from this method is approximately 150 rad/m, close to what we estimated from the radial probes. This wavenumber

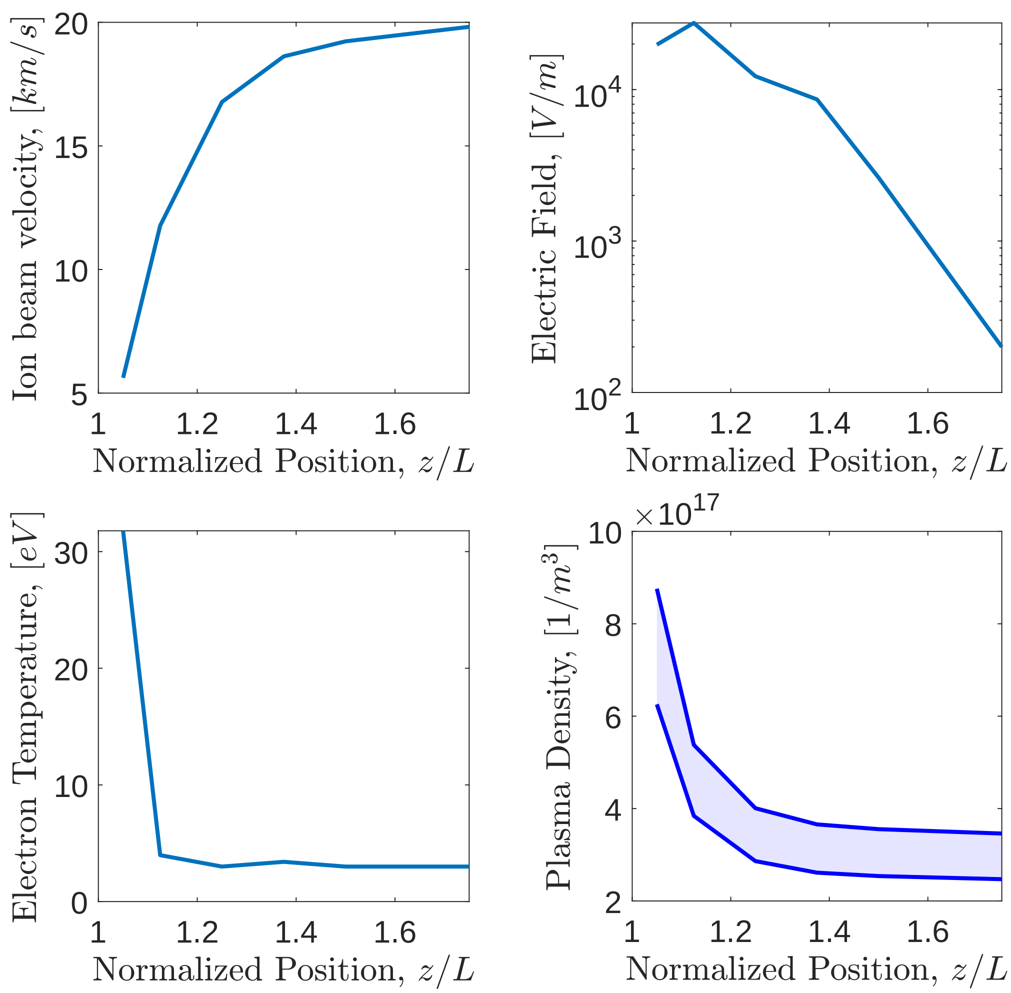

Fig. 5 Plasma properties inferred from LIF measurements. a) Ion beam velocity, b) axial electric field, c) electron temperature, and d) ion density are plotted against axial position normalized by the channel length where z/L = 1 is the exit plane of the thruster.

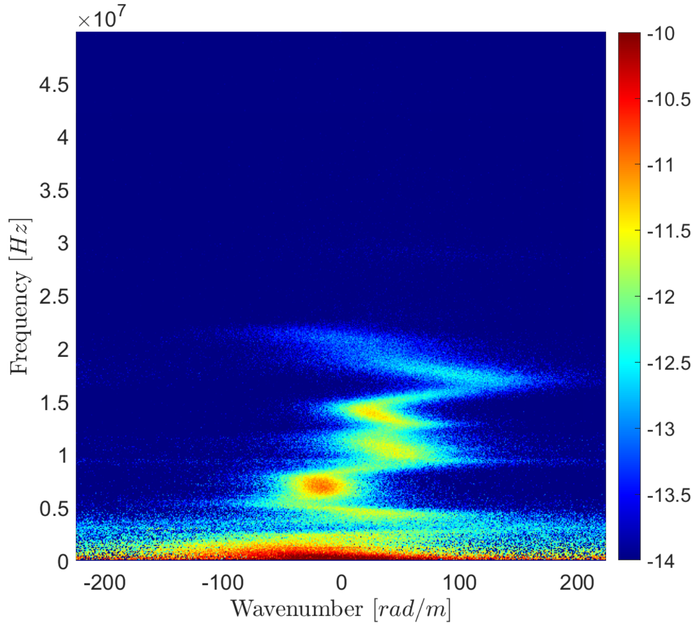

Fig. 6 Measured radial dispersion relation from experiment.

corresponds to a normalized value ($k_z \lambda_{De}$) of about 0.0075 in the acceleration region and is the value used in solving the dispersion relation when we calculate anomalous collision frequency.

C. Power spectrum of oscillations associated with EDI

The relative density oscillation amplitudes $(n_\omega/n)^2$ collected by the wave probes at various positions are shown in Figure 9. Here several distinct harmonics are visible starting at 4MHz and every ~2.7MHz thereafter. These are the frequencies corresponding to where the growth rate is a local maximum such as seen in Figure 4 and have previous been matched to EDI cyclotron resonances[23]. These are also the frequencies that show up as the high intensity zones in the Beall plots. Along the channel centerline, the oscillations are at their strongest in the acceleration zone then drops off and stays roughly constant towards the end of the near-field. This trends makes sense when considering the wave should originate in the acceleration region where its energy source, the $E \times B$ electron velocity, is largest.

D. Collision frequency

Using the methods described in Sec. II, we can calculate the anomalous collision spatial profile using the power spectrum at each location(Fig. 9 and the Gordeev function terms determined from the dispersion relation at each position (ex: Fig. 3) to evaluate Eqn. 9. This result is plotted in Figure 10 along with the collision frequency determined from LIF and the classical particle based collision frequency. Due to the uncertainty in the density profile described in Section III, the results are shown in Figure 10 as a range of possible values. For the wave driven collision frequency, we reevaluate the dispersion relation for each possible density, and for the LIF result, the spread in collision frequencies comes from the estimation of the electron velocity which depends on density (see Ref[31]).

The collision frequency profile inferred from LIF has a minimum value on the order of the classical collision frequency at the location of peak electric field ($z/L = 1.125$) then increases monotonically by over an order of magnitude going downstream. Conversely, the wave driven collision frequency is at its maximum just upstream of the peak electric field where the temperature is also high, but is approximately constant elsewhere in the plume. There is relative quantitative agreement between the two methods in the downstream near field region, but the wave driven value is almost two orders of magnitude larger than expected from LIF in the acceleration zone. The magnitude of both collision frequencies in this acceleration region makes qualitative sense. Indeed, from a macroscopic perspective, we expect that a peak in electric field should correspond to the minimum in electron collision. Similarly, since the EDI grows at the expense of the $E \times B$ drift, it also follows that the wave-driven collision should be largest at the peak electric field where

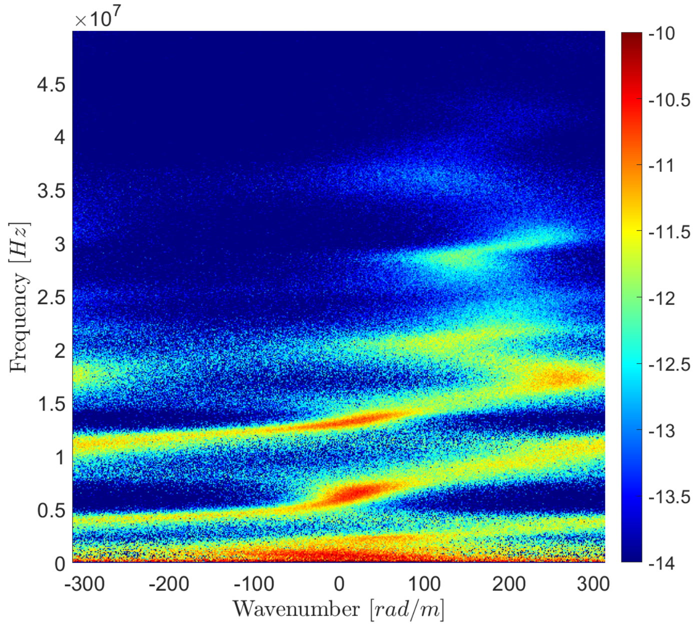

Fig. 7 Measured axial dispersion relation from experiment.

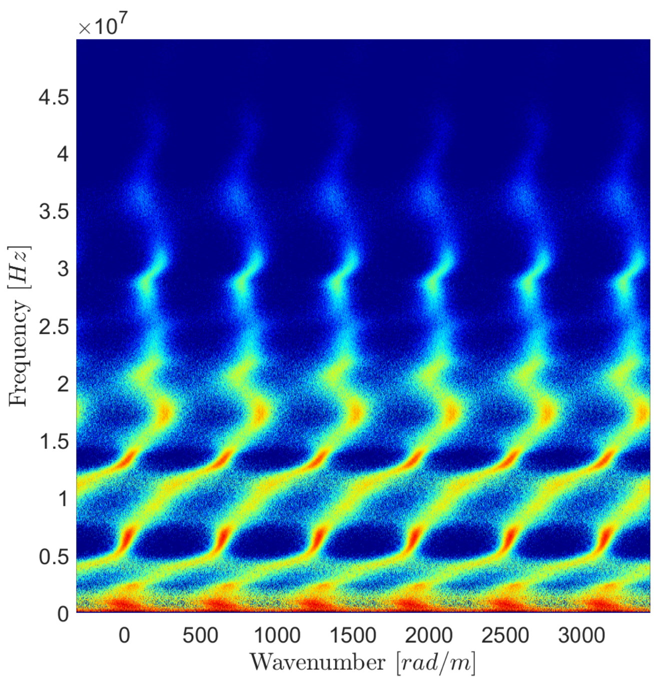

Fig. 8 Axial dispersion relation after correcting for aliasing.

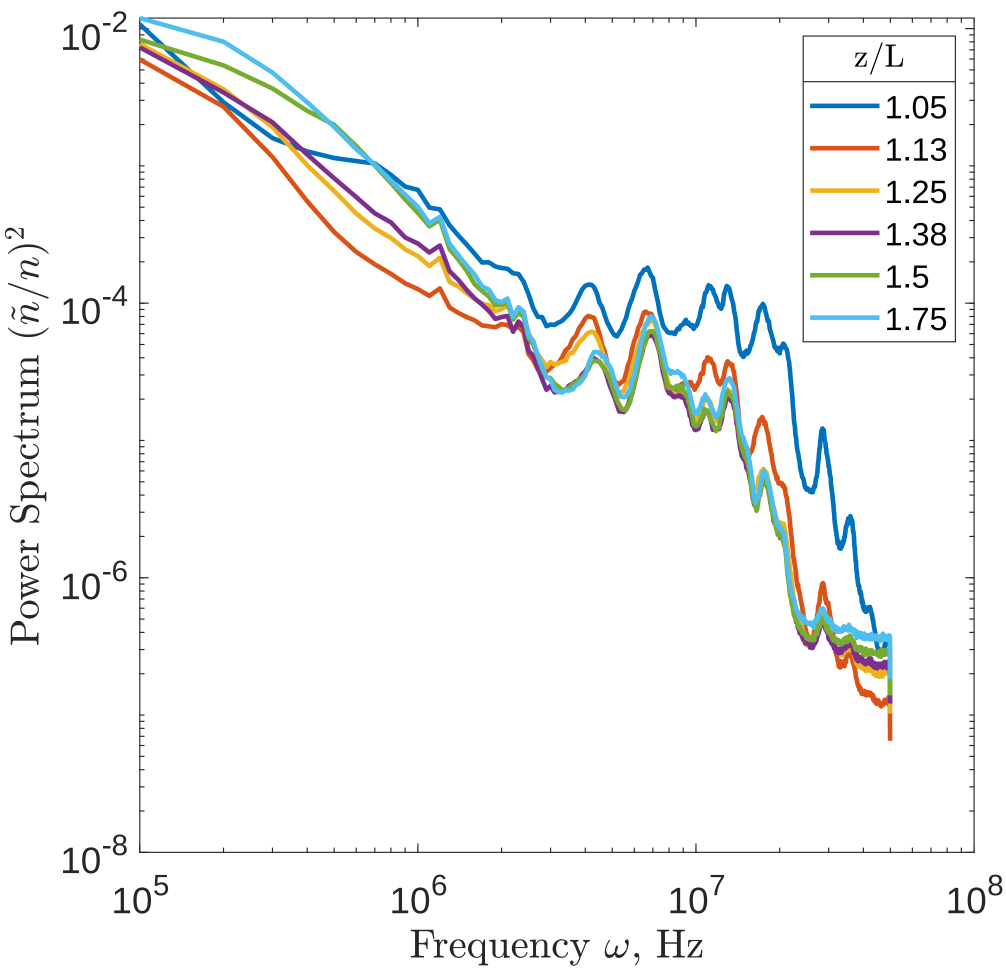

Fig. 9 Power spectrum of density oscillations as measured by wave probes at various positions in the near-field plume.

$E \times B$ is also at its maximum value. While both of these trends are thus physically plausible, it is intriguing that the anomalous collision frequency is orders of magnitude higher than the actual transport. We discuss possible reasons for this is discrepancy in the next section.

V. Discussion

The calculated anomalous collision frequency from both LIF and wave theory are found to be roughly within the same order of magnitude in the downstream near field region, but there is a divergence in the acceleration zone. This is, to our knowledge, one of the first direct confirmations that there is sufficient energy to explain the transport–in at least some regions of the plasma. With that said, the wave driven collision frequency is about two orders of magnitude larger than the value inferred from LIF, which is on the order of the classical collision frequency in this region.

The wave driven transport is predicting higher transport levels due to the high electric field and electron temperature in this region resulting in larger values of $g_i/((1+g_r)^2+g_i^2)$ in Eqn. 9. Similarly the predicted growth rate is the highest at this location due to the high electric field, even though the measured collision frequency from LIF is at its minimum. To illustrate this point we plot in Figure 11 the mean growth rate ($\bar{\gamma} = \sum_k \gamma_k / \sum_k 1$) , which is a more physically intuitive proxy for the Gordeev terms in Eqn9 against the wave energy density which we define as:

$$E_T = \sum_k T_e (\frac{n_k}{n})^2. \tag{10}$$

Both the energy density and growth rate are at their maximum near the peak electric field, which is why the calculated anomalous collision is at its maximum here.

There are a few potential reasons to explain this inconsistency between measured low collision frequency and the expected high collision frequency from theory. First, although we are assuming quasi-neutrality, simulations of the electron drift instability have shown that due to non-linear effects the amplitude of ion density oscillation can be significantly higher than the electrons[12]. Our wave probes measure ion density while the density terms in equation 9 refer to the electron amplitudes. If this effect is occurring, then wave driven collision should be uniformly lower, assuming the discrepancy between ion and electrons remains even throughout the acceleration zone. This could potentially bring the LIF and wave driven values close together in the acceleration region, but there would now be divergent behavior in the downstream near-field region.

As a second possible explanation, we note that the collision frequency in the near-field region may not fully described by just the EDI dispersion relation. Simulations have shown that the non-linear effects lead to the formation of a modified two stream instability (MTSI). The MTSI is likely non-linearly coupled to the EDI, but the theory we have developed in this work does not capture this process or its its impact on transport—particular in the lower frequency and wavenumber domain.

A third explanation for the discrepancy stems from the assumption in the EDI dispersion relation that the electrons are well represented by a Maxwellian distribution. If this is not the case, the effect of oscillations on anomalous transport can significantly change. The original work on the EDI dispersion relation by Ducrocq et al.[17] showed that the electron velocity distribution function could become distorted as the wave grows and saturates. This distortion reduces the envelope of wavelengths that can still grow and reduces the influence of the already developed wave. This effect is expected to occur more in the acceleration region where the wave forms and distorts the distribution function during its initial growth. Downstream, the electron could potentially be more Maxwellian due to the absence of the energy source for the instability, and the electrons can more easily reach equilibrium. A similar result was demonstrated by Lafleur et al.[33] using 2D PIC simulations that showed the formation of non-Maxwellian distributions resulting in growth rates significantly lower than values determined by assuming a Maxwellian as well as a reduced anomalous friction force. This same work also showed that deviation was most pronounced at the acceleration zone, whereas downstream, the Maxwellian and non-Maxwellian results were closer in agreement.

VI. Conclusion

In this paper, we performed measurements of plasma oscillations and electron mobility. We applied quasi-linear theory to relate the plasma oscillation to wave-driven electron transport. Previous work applied similar methods but could not conclusively demonstrate that the measured transport level could be attributed to wave effects. This was due to a lack of precise determination of radial wave number, which strongly determines how much the waves affect transport. Similarly, the previously employed technique for determining how the impact of each frequency largely

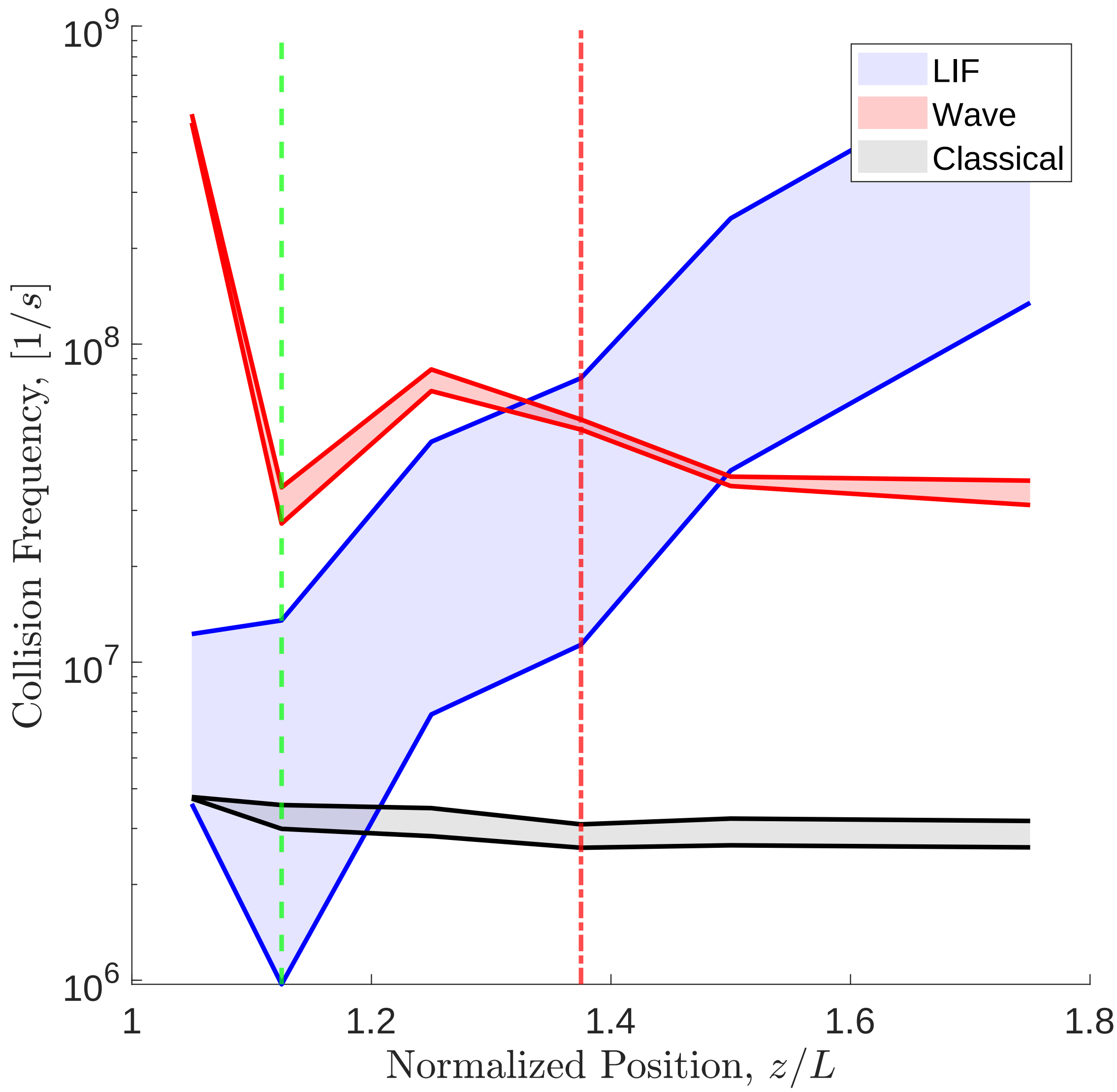

Fig. 10 Anomalous collision frequency determined from LIF and wave measurements as a function of normalized position in the Hall thruster plume. The classical collision frequency is also shown for reference. The peak electric field at $z/L = 1.125$ is denoted with a dashed green line and the peak magnetic field at $z/L = 1.375$ is denoted by the red dash dot line.

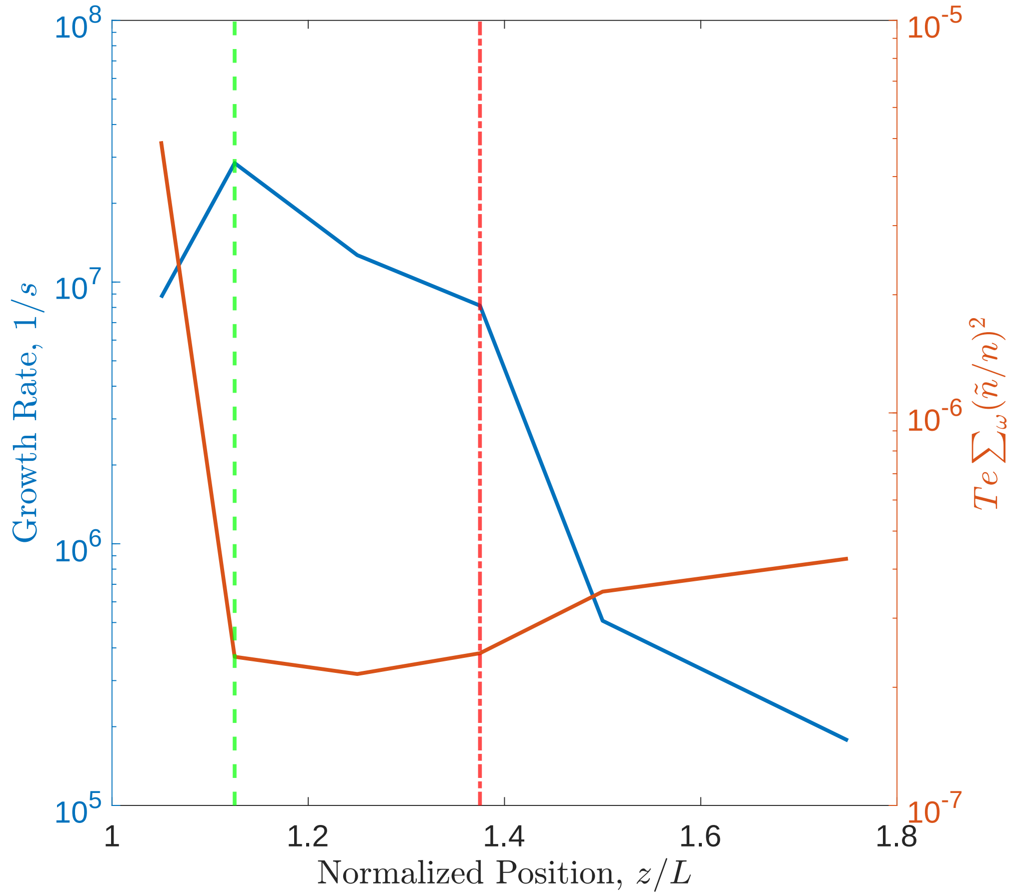

Fig. 11 Comparison between the average growth rate and total wave energy $Te\sum_\omega(\tilde{n}/n)^2$ at each position in the plume.The peak electric field at $z/L = 1.125$ is denoted with a dashed green line and the peak magnetic field at $z/L = 1.375$ is denoted by the red dash dot line.

ignored the discrete resonant nature of the instability. We improved upon this work by performing a more rigorous and precise estimation of the radial wavenumber, as well more accurately taking the resonant nature of the instability into account when calculating the wave driven transport. This significantly reduced the uncertainty our calculated collision frequencies.

Through use of quasi-linear theory the predicted collision frequency due to the electron drift instability related oscillations were shown to be in close agreement with the measured near-field electron collision frequency but significantly over-predicted the collision frequency in the acceleration zone. Possible explanations for this disagreement were proposed. Among these explanations, we have highlighted the potential role of non-equilibrium distributions in the acceleration zone impacting the momentum exchange of the wave with the background electrons. This interpretation is consistent with the conclusions of some recent, reduced dimensional kinetic simulations. Taking into account these effects will be crucial for further modelling of the EDI and its effect on electron transport in Hall thrusters.

VII. Acknowledgements

I would like to thank the entirety of the PEPL for all their aid in this experiment.

References

[1] Boeuf, J. P., "Tutorial: Physics and modeling of Hall thrusters," *Physics of Plasmas*, Vol. 121, No. 1, 2017, p. 011101.

[2] Taccognam, F., and Garrigues, L., "Latest progress in Hall thrusters plasma modelling," *Reviews of Modern Plasma Physics volume*, Vol. 3, 2019.

[3] Meezan, N. B., Hargus, W. A., and Cappelli, M. A., "Anomalous electron mobility in a coaxial Hall discharge plasma," *Physics Review E*, Vol. 62, No. 2, 2001, p. 026410.

[4] Boniface, C., Garrigues, L., Hagelaar, G. J. M., Boeuf, J. P., Gawron, D., and Mazouffre, S., "Anomalous cross field electron transport in a Hall effect thruster," *Applied Physics Letters*, Vol. 89, No. 16, 2006, p. 161503.

[5] Barral, S., Makowski, K., Peradzyński, Z., Gascon, N., and Dudeck, M., "Wall material effects in stationary plasma thrusters. II. Near-wall and in-wall conductivity," *Physics of Plasmas*, Vol. 10, No. 10, 2003, p. 4137.

[6] Gascon, N., Dudeck, M., and Barral, S., "Wall material effects in stationary plasma thrusters. I. Parametric studies of an SPT-100," *Physics of Plasmas*, Vol. 10, No. 10, 2003, p. 4123.

[7] McDonald, M. S., and Gallimore, A. D., "Parametric Investigation of the Rotating Spoke Instability in Hall Thrusters," *32nd International Electric Propulsion Conference*, 2011.

[8] Ellison, C. L., Raitses, Y., and Fisch, N. J., "Cross-field electron transport induced by a rotating spoke in a cylindrical Hall thruster," *Physics of Plasmas*, Vol. 11, No. 1, 2012, p. 013503.

[9] Boeuf, J. P., and Smolyakov, A., "Preface to Special Topic: Modern issues and applications of E x B plasmas," *Physics of Plasmas*, Vol. 25, No. 6, 2018, p. 061001.

[10] Lafleur, T., Baalrud, S. D., and Chabert, P., "Theory for the anomalous electron transport in Hall effect thrusters: I. Insights from particle-in-cell simulations," *Physics of Plasmas*, Vol. 23, 2016, p. 053502.

[11] Janhunen, S., Smolyakov, A., Chapurin, O., Sydorenko, D., Kaganovich, I., and Raitses, Y., "Nonlinear structures and anomalous transport in partially magnetized E×B plasmas," *Physics of Plasmas*, Vol. 25, No. 1, 2018, p. 011608.

[12] Janhunen, S., Sydorenko, A., Sydorenko, D., Jimenez, M., Kaganovich, I., and Raitses, Y., "Evolution of the electron cyclotron drift instability in two-dimensions," *Physics of Plasmas*, Vol. 25, No. 8, 2018, p. 082308.

[13] Ortega, A. L., Katz, I., and Chaplin, V. H., "A First-Principles Model Based on Saturation of the Electron Cyclotron Drift Instabiity for Electron Transport in Hydrodynamic Simulations of Hall Thruster Plasmas," *35th International Electric Propulsion Conference*, 2017.

[14] Boeuf, J. P., and Garrigues, L., "E x B electron drift instability in Hall thrusters: Particle-in-cell simulations vs. theory," *Physics of Plasmas*, Vol. 25, 2018, p. 061204.

[15] Héron, A., and Adam, J. C., "Anomalous conductivity in Hall thrusters: Effects of the non-linear coupling of the electron-cyclotron drift instability with secondary electron emission of the walls," *Physics of Plasmas*, Vol. 20, No. 8, 2013, p. 082313.

[16] Katz, I., Chaplin, V. H., and Ortega, A. L., "Numerical Studies of Hall Thruster Acceleration Region Electron Transport," *2018 Joint Propulsion Conference, AIAA Propulsion and Energy Forum*, 2018.

[17] Ducrocq, A., Adam, J. C., and Heron, A., "High-frequency electron drift instability in the cross-field configuration of Hall thrusters," *Physics of Plasmas*, Vol. 13, No. 10, 2006.

[18] Cavalier, J., Lemonie, G., N amd Bonhomme, Tsikata, S., Honore, C., and Gresillon, D., "Hall Thruster Plasma Fluctuations Identified as the ExB Electron Drift Instability: Modeling and Fitting on Experimental Data," *Physics of Plasmas*, Vol. 20, 2013, p. 082108.

[19] Lafleur, T., Baalrud, S. D., and Chabert, P., "Theory for the anomalous electron transport in Hall effect thrusters: II. Kinetic model," *Physics of Plasmas*, Vol. 23, 2016, p. 053503.

[20] Tsikata, S., Lemoine, N., Pisarev, V., and Gresillon, D. M., "Dispersion relation of electron density fluctuations in a Hall thruster plasma, observed by collective light scattering," *Physics of Plasmas*, Vol. 16, No. 3, 2009, p. 033506.

[21] Tsikata, S., Honore, C., Lemoine, N., and Gresillon, D. M., "Three-dimensional structure of electron density fluctuations in the Hall thruster plasma: E x B mode," *Physics of Plasmas*, Vol. 17, No. 11, 2010, p. 112110.

[22] Brown, Z. A., and Jorns, B. A., "Dispersion relation measurements of plasma modes in the near-field plume of a 9-kW magnetically shielded thruster," *35th International Electric Propulsion Conference*, 2017.

[23] Brown, Z. A., and Jorns, B. A., "Spatial evolution of small wavelength fluctuations in a Hall Thruster," *Physics of Plasmas*, Vol. 26, No. 11, 2019, p. 113504. https://doi.org/10.1063/1.5116708.

[24] Brown, Z., Dale, E., and Jorns, B. A., *Experimental Correlation between Anomalous Electron Collision Frequency and Plasma Turbulencein a Hall Effect Thruster*, 2019.

[25] Davidson, R., and Krall, N., "Anomalous transport in high-temperature plasmas with applications to solenoidal fusion systems," *Nuclear Fusion*, Vol. 17, 2018, p. 1313.

[26] Tsikata, S., "Small-Scale Electron Density Fluctuations in the Hall Thruster, Investigated By Collective Light Scattering," Ph.D. thesis, Ecole Polytechnique X, 2009.

[27] Hofer, R. R., Cusson, S. E., and Lobbia, R. B., "The H9 Magnetically Shielded Hall Thruster," *35th International Electric Propulsion Conference*, 2017.

[28] Cusson, S. E., Hofer, R. R., Lobbia, R. B., Jorns, B. A., and Gallimore, A., "Performance of the H9 Magnetically Shielded Hall Thrusters," *35th International Electric Propulsion Conference*, 2017.

[29] Mikellides, I. G., Katz, I., Hofer, R., and Goebel, D., "Magnetic shielding of walls from the unmagnetized ion beam in a Hall thruster," *Applied Physics Letters*, Vol. 102, No. 2, 2013, p. 023509.

[30] Pérez-Luna, J., Hagelaar, G. J. M., Garrigues, L., and Boeuf, J. P., "Method to obtain the electric field and the ionization frequency from laser induced fluorescence measurements," *Plasma Sources Science and Technology*, Vol. 18, No. 3, 2009, p. 034008.

[31] Dale, E. T., and Jorns, B. A., "Non-invasive time-resolved measurements of anomalous collision frequency in a Hall thruster," *Physics of Plasmas*, Vol. 26, No. 1, 2019, p. 013516. https://doi.org/10.1063/1.5077008.

[32] Beall, J. M., Kim, Y. C., and Powers, E. J., "Estimation of wavenumber and frequency spectra using fixed probe pairs," *Physics of Plasmas*, Vol. 53, 1982, p. 3933.

[33] Lafleur, T., Chabert, P., and Bourdon, A., "Anomalous electron transport in Hall-effect thrusters: Comparison between quasilinear kinetic theory and particle-in-cell simulations," *Physics of Plasmas*, Vol. 25, 2018, p. 061202.